33RD CONGRESS
OF THE INTERNATIONAL COUNCIL
OF THE AERONAUTICAL SCIENCES
STOCKHOLM, SWEDEN, 4-9 SEPTEMBER, 2022

ICAS 2022 SWEDEN

STRESS AND ENERGY RELEASE RATE INFLUENCE ON ICE SHEDDING WITH RESONANT ELECTROMECHANICAL DE-ICING SYSTEMS

G.Gastaldo[1], V.Palanque[1,2], M.Budinger[3] & V.Pommier-Budinger[1]

[1]ISAE-SUPAERO, University of Toulouse, 10 Avenue Edouard Belin, 31400 Toulouse, France
[2]ONERA/MFE, University of Toulouse, F-31055 Toulouse - France
[3]Institut Clément Ader (ICA), University of Toulouse, INSA, ISAE-SUPAERO, MINES ALBI, UPS, CNRS

Abstract

Electromechanical resonant de-icing systems provide a low-power solution to avoid ice accretion on aircraft. These systems rely on actuators, e.g. piezoelectric transducers, which generate high level of stresses within the ice by inducing vibrations in the substrate. This ultimately leads to bulk or adhesive failure of the ice layer and eventually to ice shedding. In order to design an efficient ice protection system it is of utmost importance to evaluate fracture propagation mechanisms. Three key parameters play a role in this phenomenon: the tensile and shear strengths and the critical energy release rate. This paper proposes an evaluation of the influence of stress and energy release rate on cohesive and adhesive fracture propagation for both flexural and extensional modes through numerical analyses. The results are verified by experimental tests, highlighting the relevance of the numerical method proposed in this study.

Keywords: Electromechanical de-icing, Fracture mechanics, Brittle fracture, Tensile strength, Shear strength, Energy release rate

Nomenclature

CC	Coupled Criterion
CZM	Cohesive Zone Model
FEM	Finite Element Method
LEFM	Linear Elastic Fracture Mechanics

1. Introduction

Icing constitutes a severe issue for aviation [1]. Ice can either deposit on the structure on the ground or during flight. On the ground, snow or freezing rain can settle on the aircraft, leading to the formation of snow, ice, or a combination of these two. In-flight icing occurs when an aircraft flies through clouds in which supercooled droplets are suspended. The droplets impact on the aircraft surfaces and freeze. The accreted ice is responsible for the changes in the airfoil geometry, which alter the aerodynamic properties of the wing, leading to severe performance degradation and safety threats [2] [3].

Ice protection systems are thus necessary to ensure a safe and efficient operation of the aircraft. For large jet engine aircraft, thermal systems are the most adopted solutions, they provide heat to the critical surfaces. This can either prevent ice formation, or it can provide a solution when ice is already

present on the structure. They require either a significant power, retrieved by the bleed of hot air from the engines or a great amount of energy, provided by the electric grid for electrothermal solutions [4]. Due to the high power supply required for these thermal ice protection systems, alternative strategies are studied.

Mechanical de-icing systems are less energy-demanding solutions. They induce significant stresses in the ice, leading to its failure and eventually to ice shedding. Commonly employed in regional and smaller aircraft, pneumatic systems are low energy consuming solutions. Conversely, they have a significant impact on the aerodynamics of the aircraft and require regular maintenance due to the poor material endurance [5]. In recent years, electromechanical systems employing piezoelectric actuators have gained increasing interest due to their potential in terms of weight and energy savings. They excite the surface covered by ice with vibrations, which generate high stresses within the ice, leading to its failure [6], [7].

Several studies have been carried out to evaluate the feasibility and the efficiency of electromechanical ice protection systems. Ramanthan et al. propose the use of electromechanical de-icing of helicopter blades in a range of frequencies around 1 Megahertz [8]. Ice melting was witnessed at the ice/substrate interface. On the other hand, some works explore the effectiveness of these systems with low frequency modes (below 1000 Hz) [9], [10], [11]. The majority of the studies related to electromechanical ice protection systems are carried out in the range of kilohertz frequencies. Palacios et al. led the study of de-icing systems at frequency around a few tens of kilohertz on both plates and on leading edges. Ice shedding occurred instantaneously [12], [13]. Rotor icing testing under the effects of ultrasonic excitation was conducted as well by Overmeyer et al. [14].

Other studies have given attention to the link between the electromechanical de-icing systems and the physical mechanisms leading to fracture propagation phenomena. The initiation of icing fracture by means of piezoelectric actuators was investigated by Pommier-Budinger et al. in [15], where voltages and currents required to initiate cohesive fractures are computed numerically and experimentally validated. Several studies were also conducted to acknowledge ice fracture propagation mechanisms. Sommerwerk used Cohesive Zone Model (CZM) to study numerically the bulk ice failure process on thin plates [16] and leading edges [17]. In both papers, the method was combined with an adhesive de-icing criterion based on shear stresses. In [18], CZM was introduced to describe the interface behavior of the plate and ice layer. Marboeuf et al. proposed a model based on phase-field variational approach to fracture [19], which, unlike previous studies, does not require the a priori knowledge of the fracture propagation path. In [20], the energy balance approach is used to study ice failure in modal analyses. This method is fast to compute and does not require the traction-separation law needed when using CZM. To accurately predict the effects that lead to the crack onset, the use of a coupled criterion (CC) was firstly introduced by Leguillon in the study of adhesively bonded joints [21] [22]. According to this method, fracture initiation must meet both energy release rate and stress criteria. Later, Golovin et al. [23] evaluated the influence of these criteria to assess the adhesive fracture propagation, highlighting the existence of two distinct shedding mechanisms according to different ice layer dimensions.

The goal of this paper is to further investigate the mechanisms of fracture initiation and propagation in the case of resonant de-icing systems, by evaluating the influence of stress and energy release rate on the two types of resonant modes identified in [20], i.e. flexural and extensional modes. The criteria and method used in this paper to assess the crack initiation and propagation are respectively described in section 2.and in section 3. Three criteria based on both tensile and shear stresses and on the energy release rate are established to allow the analysis of the influence of these quantities in de-icing mechanisms. In section 4.the three criteria are computed from 2D finite element simulations and are analyzed to predict the mechanisms leading to the existence of cohesive fractures in the ice and to the initiation of adhesive fractures at the ice/substrate interface. In section 5. the criteria are computed from 3D finite element analyses simulating the propagation of adhesive fractures in different configurations and are analyzed to predict the mechanisms involved in the complete ice debonding. These numerical results are confronted to experimental results and verified in section 6.

2. Criteria for analyzing fracture initiation and propagation

Two different kinds of fractures can occur when studying the de-icing mechanism by an electromechanical ice protection system: cohesive fractures (or bulk fracture) occurring within the block of ice, and adhesive fractures, occurring at the interface between the ice and the substrate. Cohesive fractures do not always appear in the de-icing process and, if they occur without adhesive fractures, they do not allow ice shedding since the ice can stick to the surface on which it is accreted. Adhesive fractures are necessary for ice debonding. In this paper, the objective is to study the complete debonding of ice from a substrate. It is thus important to understand the mechanisms involved in the initiation and propagation of adhesive fractures. It is also necessary to understand the conditions of appearance of cohesive fractures since, if they occur, those last ones play a role in the initiation and propagation of adhesive fractures by altering the stress distribution and the modal displacements.

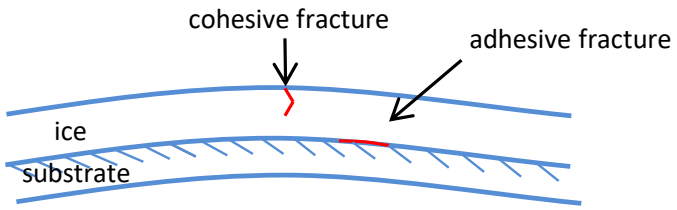

Figure 1 – Cohesive and adhesive failure

When dealing with fracture propagation in brittle materials, linear elastic fracture mechanics (LEFM) is often used. It relies on the computation of the strain energy release rate G. This theory considers a pre-existing sharp crack within the system, thus fracture initiation is not taken into account.
According to Golovin et al.[23], the delamination of ice due to adhesive fractures can be obtained by either exceeding the allowable energy release rate $G \geq G_c$ or, in the case of smaller ice blocks, by exceeding the critical shear stress value over the interface $\tau_{xy} \geq \tau_c$. There is a critical bonded length l_c at which a transition between these two modes of failure occurs.
Concerning cohesive fractures in ice, as the ice thickness is small, the fracture mechanism relies only on the exceeding of the critical tensile stress value.

2.1 Tensile stress criterion

The cohesive stress condition is based on the characteristic value of critical tensile stress σ_c of the ice. Rankine theory specifies that cohesive fractures appear in brittle material if:

$$\sigma_I \geq \sigma_c \tag{1}$$

where σ_I represents the principal stress i.e. tensile stress in the ice.

2.2 Shear stress criterion

The adhesive stress condition is based on the characteristic value of critical shear stress τ_c of the studied interface. It is assumed for the following studies in this paper that full delamination occurs when the following condition is respected:

$$min(\tau_{xy}) \geq \tau_c \tag{2}$$

where $min(\tau_{xy})$ represents the minimum shear stress over the resulting interface.

2.3 Energy release rate criterion

The energy condition relies on the critical energy release rate (or toughness) value G_c. This value can be characteristic of the considered material if bulk fracture is considered, whereas for adhesive

fracture it is dependent on the studied interface. According to fracture mechanics theory, crack propagation is obtained when a certain amount of stored elastic energy is released to form a crack.
The energy release rate is given by:

$$G = -\frac{1}{b}\frac{dU}{da} \tag{3}$$

where dU is the differential decrease of potential energy, da is the differential crack length increment and b is the specimen width.
The fracture propagates if the released energy is equal to or greater than the critical value of G, thus expressed as $G \geq G_c$.

2.4 Mechanical properties of the ice

To assess ice failure with accuracy, it is necessary to attribute the correct mechanical properties to ice, knowing that the experiment verification will be carried out with freezer ice. Many experiments were conducted to measure the critical shear strength [24] [25] [26], however studies show high discrepancy in their results. This can be due to the important scattering in the ice mechanical properties according to the type of ice, but also by the difficulty to load the interface experimentally with pure shear stress [27]. The value of 0.5 MPa for the critical shear strength is selected for the computations of this article as it is commonly used in the literature for freezer ice and standard metal surfaces as shown in [28].
Ice tensile strength value is in the range between 0.7 MPa to 3.1 MPa [29, 30, 31, 32, 33]. This parameter is highly influenced by temperature, strain rate, tested volume, and ice grain size. A conservative tensile strength value of 3 MPa is hereafter adopted.
According to bibliography, the critical energy release rate at the interface of the ice is highly dependent on the interface properties such as its material, its roughness but also the ice properties themselves [34]. Andrews et al.[29] estimated that a mean value of the critical value of the energy release rate G_c is 1.0 J/m². This value commonly used in the literature will be used in this article.
Finally, table 2 summarizes all the values adopted for the critical strengths and the critical energy release rate considered for the computations performed in this study.

Table 2 – Critical stress and energy release rate selected for the study

	Tensile stress (MPa)	Shear stress (MPa)	Energy release rate (J/m²)
Critical values	3.0	0.5	1.0

3. Method for analyzing fracture mechanisms

3.1 Principle of the method for analyzing fracture mechanisms

For flexural and extensional modes, the method for analyzing the mechanisms involved in the generation of fractures consists in comparing the amplitudes required to initiate a fracture by exceeding the critical stress value and the amplitude required to initiate propagation by exceeding the critical energy release rate.
Based on the method described in [35, 36], the amplitude required to initiate a cohesive fracture based on the tensile stress criterion is defined by (4):

$$x_{r\sigma} = \frac{\sigma_c}{\sigma_{mod}} x_{mod} \tag{4}$$

with σ_c the critical tensile stress of ice, σ_{mod} and x_{mod} respectively the modal tensile stress and the modal displacement.
Similarly, the amplitude required to initiate an adhesive fracture based on the adhesive stress criterion is defined by (4):

$$x_{r\tau} = \frac{\tau_c}{min(\tau_{mod})} x_{mod} \tag{5}$$

with τ_c the critical shear stress of ice, τ_{mod} and x_{mod} respectively the modal shear stress and the modal displacement.
Finally, the amplitude required to initiate fracture propagation based on an energy release rate criterion is defined by (6):

$$x_{rG} = \sqrt{\frac{G_c}{G_{mod}}} x_{mod} \tag{6}$$

with G_c the critical value of the energy release rate and G_{mod} and x_{mod} respectively the modal energy release rate and the modal displacement. In the case of flexural mode, the displacement is retrieved in the orthogonal direction to the plate, whereas for an extensional mode, the displacement is the lateral displacement of the plate.

In the next section, results are analyzed, knowing that a smaller displacement implies a greater ease to generate fractures. If $x_{rG} < x_{r\sigma}$ or $x_{rG} < x_{r\tau}$, the de-icing mechanism is said to be energy release rate dominant, otherwise it is said to be stress dominant.

3.2 Implementation of the method and study case

In this paper, the study is carried out numerically on a 130 mm-long, 50 mm-wide and 1 mm-thick titanium plate, in free conditions, covered by a 2 mm thick ice layer having the same width as the plate but not necessarily the same length. To facilitate experimental verification, the considered ice is freezer ice, since making ice in a freezer allows getting a constant ice layer and makes the comparison of theoretical and experimental results easier. The mechanical properties of the model's materials are given in table 3. In order to reduce computation time, the plate model is reduced to a symmetric 2D model using the plain strain hypothesis, thus results will be given in the range [0-65 mm]. Moreover, to enable accurate computation of the stresses at the interface, a refined mesh is defined, and the meshing convergence is verified. The study will be carried out for the first flexural mode and the first extensional mode of the structure with ice.

Table 3 – Material mechanical properties for the Finite Element Analysis

	Density (kg/m3)	Young's Modulus (GPa)	Thickness (mm)
Substrate	4370.0	110.0	1.0
Ice	850.0	7.0	2.0

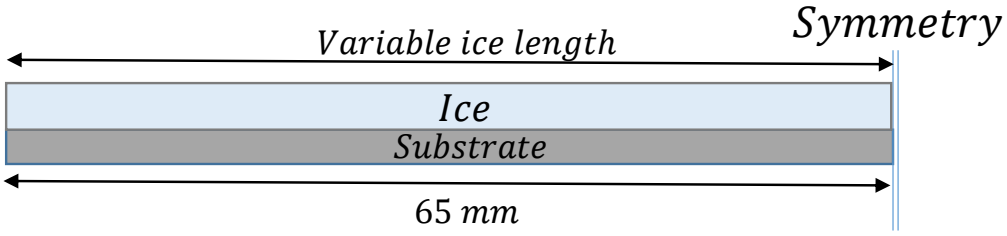

Figure 2 – Reduced numerical model

First, the nodal stresses values are retrieved. Then, the energy release rate is numerically computed as defined in [36]. An artificial crack is propagated and the elastic strain energy of the structure is retrieved for given propagation steps i. The energy release rate value is then computed using the standard formula (7):

$$G = -\frac{1}{b}\frac{\delta U}{\delta a} = \frac{1}{b}\frac{U_i - U_{i+1}}{a_{i+1} - a_i} \tag{7}$$

with b the width of the model, a the length of the crack and U the elastic strain energy of the structure. Finally, once the σ and G values have been obtained, the amplitudes of (4), (5) and (6) are computed, which allows the analysis of fracture propagation mechanisms.

4. Analysis of the mechanisms leading to initial adhesive fractures

A first study is carried out here on blocks of ice of different lengths, from a few millimeters long up to the entire length of the substrate, i.e. 65 mm, to determine, according to the size of the block of ice, the possible mechanisms for the initiation of fractures.

On an undamaged configuration, as explained in section 2, it is possible:

- either to generate cohesive fractures in the ice thickness by tensile stress,
- or to generate adhesive cracks at the interface by the energy release rate (energy release rate dominant mechanism),
- or to debond the ice thanks to high shear stress over the interface (shear stress dominant mechanism).

Figure 3 shows the locations of the initiation of the fractures depending on the fracture mechanisms in the case of excitation of the first mode of flexion or of extension.

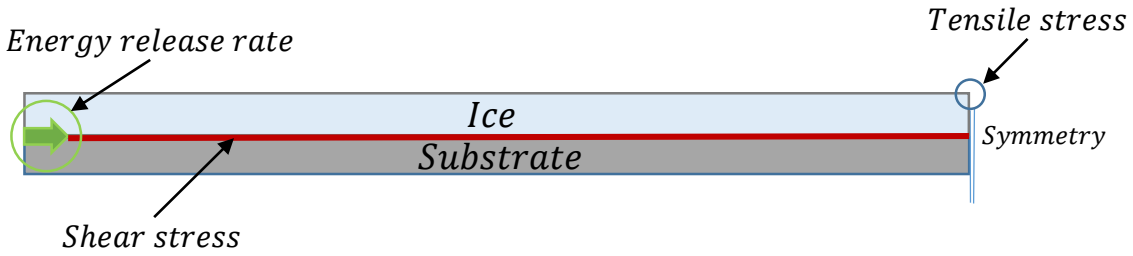

Figure 3 – Fracture initiation mechanisms on undamaged configuration

Figure 4 shows the amplitudes required to trigger each of the mechanisms described in figure 3 and the influence of the length of the block of ice in the mechanism occurrence. The values are computed for the same initial configuration without cracks for different ice lengths in the range of [2.5 - 65 mm] with a 2.5 mm step. In the case of energy release rate dominant mechanism, X_{cG} represents the amplitude required for the very first millimeters of adhesive fracture starting from the edges of the interface.
For the flexural mode configuration (figure 4(a)), the intersection of the curves $X_{r\sigma}$ and X_{rG} highlights a critical ice length, which shows how the length of the ice influences the mechanism at work. If a block of ice layer is longer than l_c= 25 mm, a cohesive crack will appear in the middle of the plate, at the antinode of the mode. For a shorter ice layer, the cohesive fracture does not prevail and delamination, characteristic of adhesive fracture, will occur starting from the edges. The curve $X_{r\tau}$, of much higher amplitude than the two other curves, indicates that the shedding of ice due to shear stress is unlikely for this configuration based on the excitation of the first mode.
For the extensional mode configuration (figure 4(b)), for small dimensions of the block of ice (below l_c), the dominant effect will be the total debonding on the interface due to shear stress. For slightly longer ice blocks, according to the critical values used, both cohesive and adhesive fractures can occur. Finally, for ice blocks with large dimensions, a cohesive fracture will appear, prevailing over adhesive delamination from the edges.
When the cohesive crack is created, whatever the mode, flexion or extension, the initiation of adhesive fractures starts from the cohesive fractures, as described in [35].

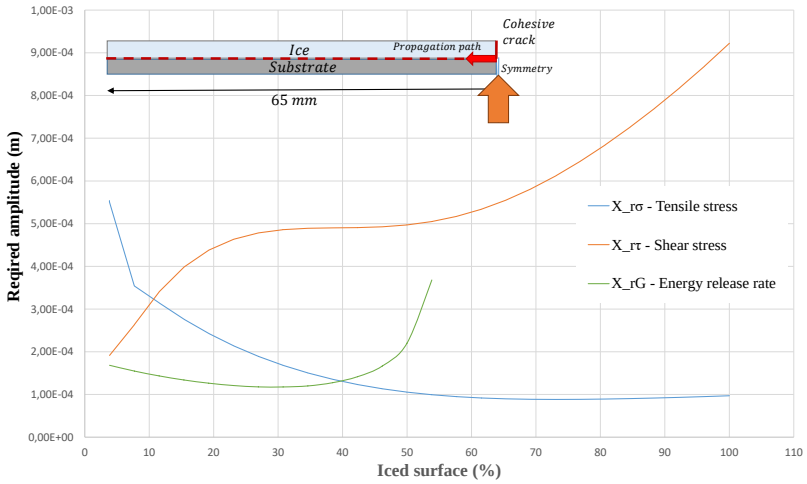

(a) *Flexural mode*

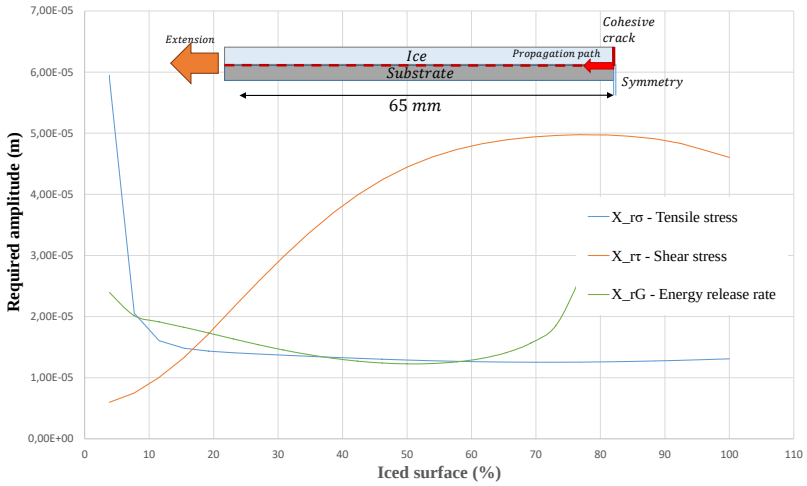

(b) *Extensional mode*

Figure 4 – Influence of the ice length on the amplitude required to achieve cohesive and adhesive failure

Finally, four different configurations can be defined:

- Excitation of a structure largely covered by ice and excited by flexural modes, which leads to cohesive fractures in the ice and then adhesive fractures at the ice/structure interface starting from the cohesive fractures.
- Excitation of a structure partly covered by ice and excited by flexural modes, which does not lead to cohesive fractures in the ice but to adhesive fractures at the ice/structure interface starting from the edges of the ice block.
- Excitation of a structure quite largely covered by ice and excited by extensional modes, which can lead to fractures by tensile stress or by stored energy.
- Excitation of a structure poorly covered by ice and excited by extensional modes, for which shear stress generates ice delamination.

Figure 5 summarizes the configurations under study.

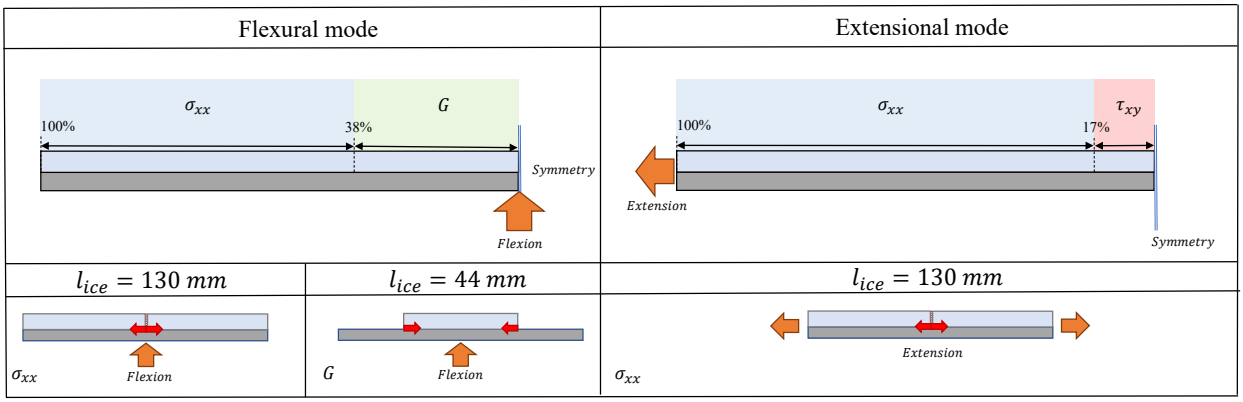

Figure 5 – Fracture initiation configurations according to ice length

5. Analysis of mechanisms involved in adhesive fracture propagation

This section focuses on the propagation of adhesive fractures, since they are essential in ice debonding by electromechanical de-icing systems. The analysis is again performed for the first flexural mode or for the first extensional mode.

In section 4. the stress and energy release rate criteria have been used to highlight configurations with different de-icing mechanisms for the initiation of adhesive fractures and to assess the existence of cohesive fractures in the ice before ice delamination at the interface in some configurations. It has been shown that the de-icing mechanisms depend on the length of the ice block. In this section, analyzes of these configurations are carried out to study the different mechanisms for obtaining a complete detachment of the ice. The challenge is to know whether the debonding is achieved by shear stresses or by released energy, or by both mechanisms. This better understanding of the mechanisms will make it possible to better design electromechanical ice protection systems.

5.1 Flexural mode

As mentioned in section 4. de-icing mechanisms depend on the size of the ice block. First, it is analyzed the mechanism leading to a cohesive fracture which is initiated in the middle of the ice starting from the upper surface. The crack then propagates through the entire thickness of the ice, finally resulting in an outward propagation of the adhesive crack. To study this mechanism, ice length must be higher than l_c (equal to 25 mm for the case under study). An ice length of 65 mm is used (over the whole plate) to analyze ice debonding under the most difficult circumstance. In figure 6, the critical amplitude required to propagate an adhesive fracture at the ice/substrate interface after the cohesive fracture is computed according to the length of the adhesive crack, from the first millimeter of crack to a complete crack. As the crack extends, the amplitude required to propagate increases. The computation of the amplitude is performed according to the two criteria (shear stress and energy release rate). In this configuration, the amplitude computed for the energy release rate mechanism is always below the amplitude computed for the shear stress mechanism, which shows that is this first one is the only one at work, regardless of the crack length.

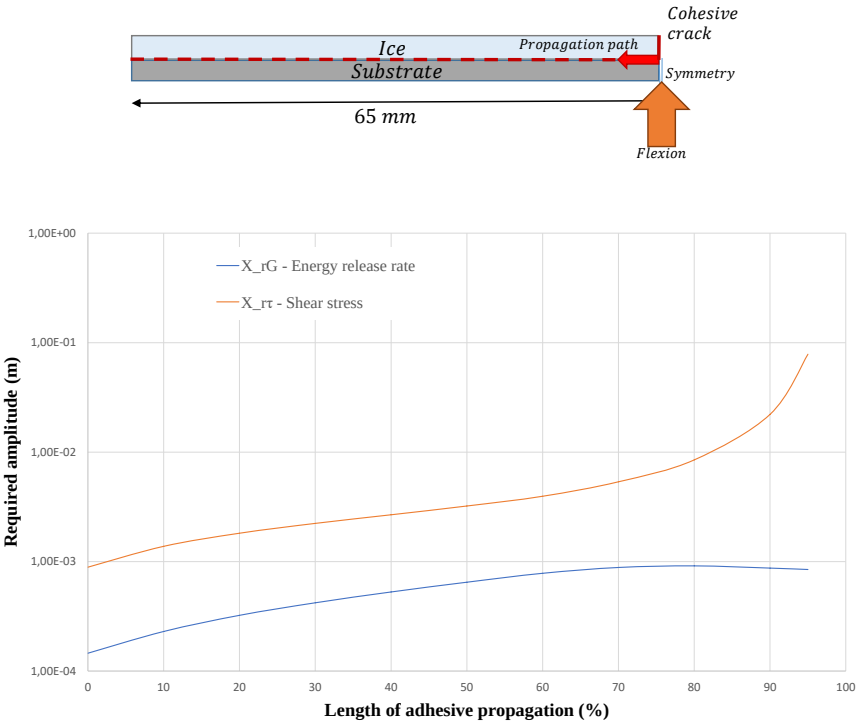

Figure 6 – Critical amplitude required for adhesive debonding according to energy release rate and shear stress - Case of the first flexural mode with a large ice block

Secondly, the mechanism with no initial cohesive fracture is analyzed. In this case, the ice debonding at the interface starts from the edges of the ice block. This mechanism occurs for lengths of ice blocks under l_c (here 25 mm). In order to study this kind of adhesive debonding, the case of a 22 mm long ice block is considered. Figure 7 gives the critical amplitude required to propagate an adhesive fracture at the ice/substrate interface according to the shear stress and energy release rate criteria. It shows that the energy release rate mechanism is dominant at the beginning of the debonding and propagates inward upon reaching 80% of delamination. After this limit, the remaining ice can break by shear stress, leading to a complete debonding of the ice.

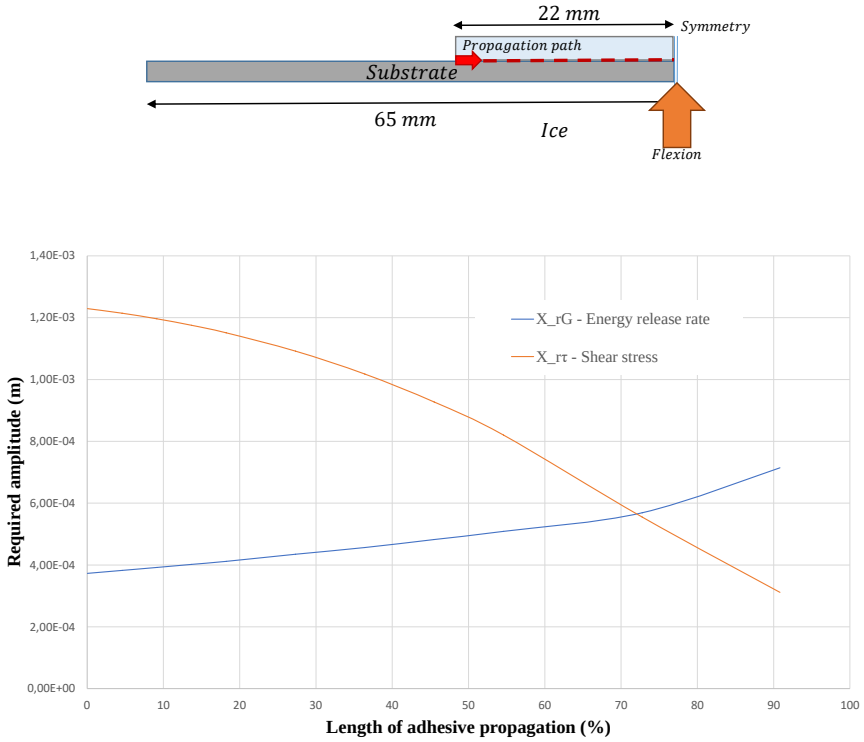

Figure 7 – Critical amplitude required for adhesive debonding according to energy release rate and shear stress - Case of the first flexural mode with a small ice block

5.2 Extensional mode

For extensional modes, there are also two configurations according to the length of ice block.
The configuration with a small ice block (under l_c) is not to be analyzed here since this is a simple case where the complete debonding can be achieved by applying shear stress.
For blocks of ice of sufficient lengths on which cohesive fractures do appear first, computations are run to observe the mechanism at work for getting complete debonding after the occurrence of the cohesive crack. Figure 8 gives the amplitudes for propagating adhesive fractures computed according to the two criteria (shear stress and energy release rate) for the plate completely covered by ice. For the first steps of the propagation, the crack propagates thanks to a high level of energy release rate. According to the critical values selected for the case 3, the crack propagates up to 70% of the total length under energy release rate dominant mechanism. Finally, with the total interface length being significantly reduced, the last 30% can be debonded by shear stress.

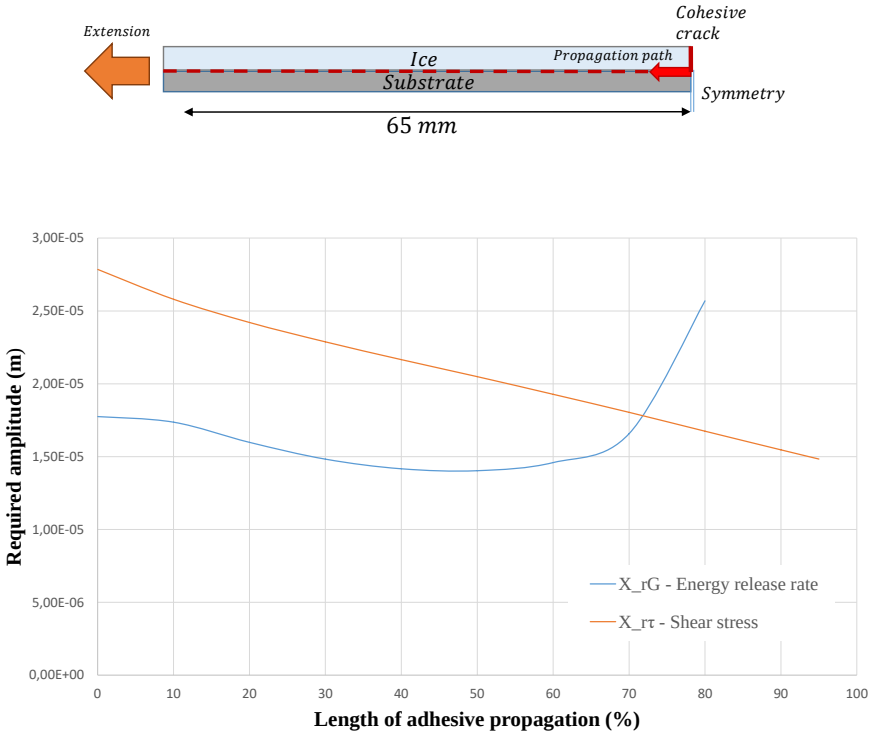

Figure 8 – Critical amplitude required for adhesive debonding according to energy release rate and shear stress - Case of the first extensional mode with a large ice block

6. Experimental verification

6.1 Specimen definition

An experimental procedure is designed to verify the results obtained thanks to the 2D modal finite element computations. A titanium substrate of dimensions 130 x 50 x 1 mm^3 is machined and equipped with piezoceramics (PIC 181) of dimensions 70 x 17 x 1 mm^3. Figure 9 details the positions of the transducers.

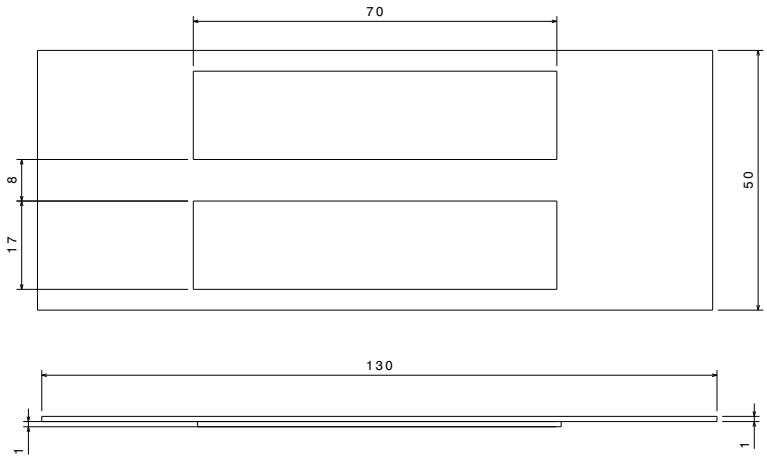

Figure 9 – Specimen dimensions

The ice is accreted in a freezer by spraying demineralized water on the substrate. The substrate is pre-cooled at the freezer temperature of -20 °C. The water is injected, creating a liquid layer on the

substrate. The volume is adjusted until the desired ice thickness is reached.

6.2 Long ice block under flexural load

In this configuration, it is predicted that the debonding is going to occur gradually, as the adhesive crack mechanism appears to be energy release rate dominant. The experimental tests confirm the numerical prediction. By exciting the first flexural mode of the structure, a cohesive crack appears at the center of the ice block. Then, the adhesive crack propagates from the previously created cohesive crack (whitish ice area).

Figure 10 – Example of adhesive propagation with a long ice block using first mode of bending and increasing voltage (150 V, 200 V and 250 V)

According to the 2D analysis, the adhesive debonding is induced by exceeding the critical energy release rate (see figure 6). This is also confirmed by a 3D numerical analysis. In the 3D simulation, the piezoelectric ceramics are taken into account contrarily to the 2D simulation. It is important to notice that the presence of piezoelectric transducers influences the curve of the x_G amplitudes as shown in figure 11. In fact, it is possible to notice that when the fracture propagation reaches the external edge of the transducer, there is a significant drop in the amplitude required to further separate the ice, thus giving a more detailed information about the energy released from the system.

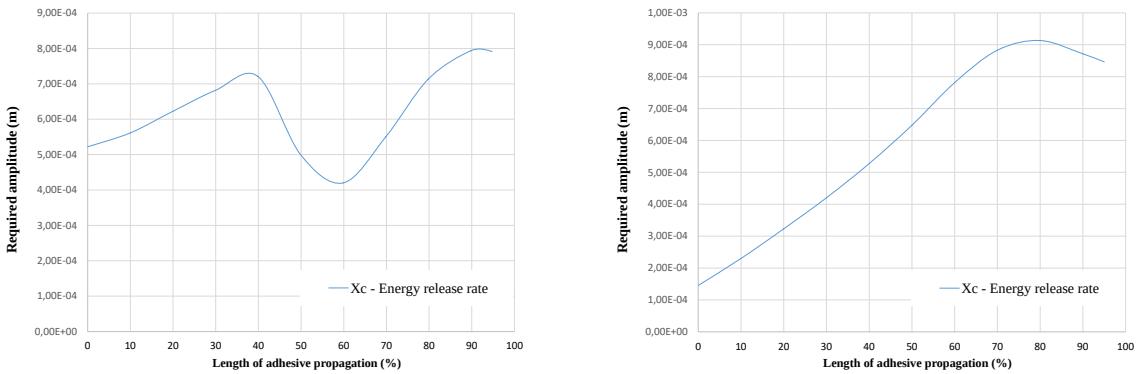

(a) *2D analysis* (b) *3D analysis*

Figure 11 – Amplitude x_G

6.3 Short ice block under flexural load

In this configuration, it is predicted that the debonding is going to begin from the edge of the interface to the center of the plate, without cohesive fractures. The adhesive crack mechanism is, at first,

energy release rate dominant and appears to become stress dominant at the end of the crack propagation. The dimensions of the ice of the finite element model are adjusted, and the computations are run.
First, a 44 mm-long ice layer was accreted on the plate, with a thickness of 2 mm. Based on figure 4 (a), the expected mechanism is a purely adhesive propagation from the edges to the center of the plate. As shown in figure 12, the adhesive propagation occurs together with cohesive cracks in the middle.

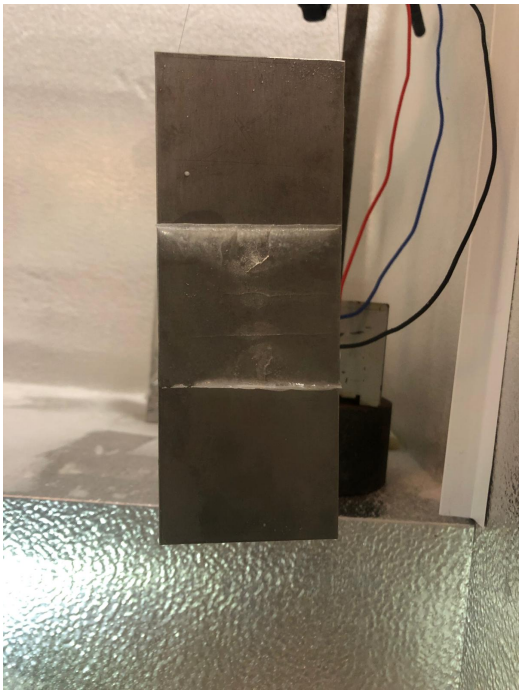

Figure 12 – Example of ice failure for a 44 mm-long ice block using the first flexural mode (200 V)

Thus, the plot correlating the ice length with the amplitude of the methods is computed again for a 3D model, which also considers the influence of piezoelectric transducers (figure 13). Compared to the 2D model, the amplitude required to generate a cohesive crack can occur for shorter ice layers.
Furthermore, the 3D model shows that the amplitudes required to initiate a cohesive fracture or an adhesive one are almost the same for a block of ice of 40 mm. Hence, the combination of these two effects can occur, leading to an incorrect prediction of the fracture mechanism at work in the 2D model.

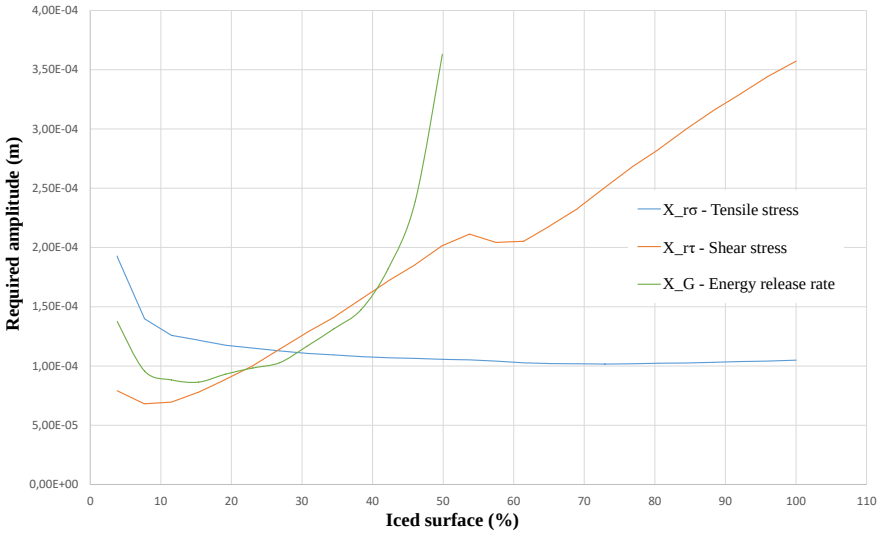

Figure 13 – Influence of the ice length on the amplitude required to achieve cohesive and adhesive failure - 3D study

The flexural mode is therefore studied for a plate with a smaller block of ice accreted on top. A length of 25 mm was chosen for the ice layer, and for this dimension a purely adhesive separation is expected according to figure 13. The adhesive fracture propagation amplitude is evaluated thanks to a 3D numerical analysis (figure 14). As presented in this figure, when the ice is undamaged, fracture is expected to propagate first by exceeding the critical value of energy release rate. When reaching approximately 60% of fracture propagation, the fracture propagates instantaneously by exceeding the critical shear stress value. The aforementioned process has been witnessed during the experimental test. As predicted from the 3D study, the propagation starts from the edges of the plate and the ice is debonded without the presence of any cohesive fracture (figure 15).

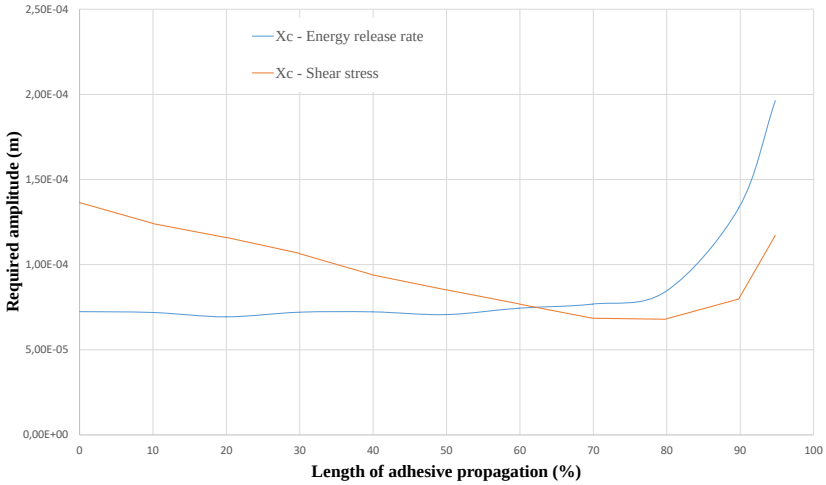

Figure 14 – Critical amplitude required for adhesive debonding according to energy release rate and shear stress - Case of the first flexural mode with a 25 mm-long ice block

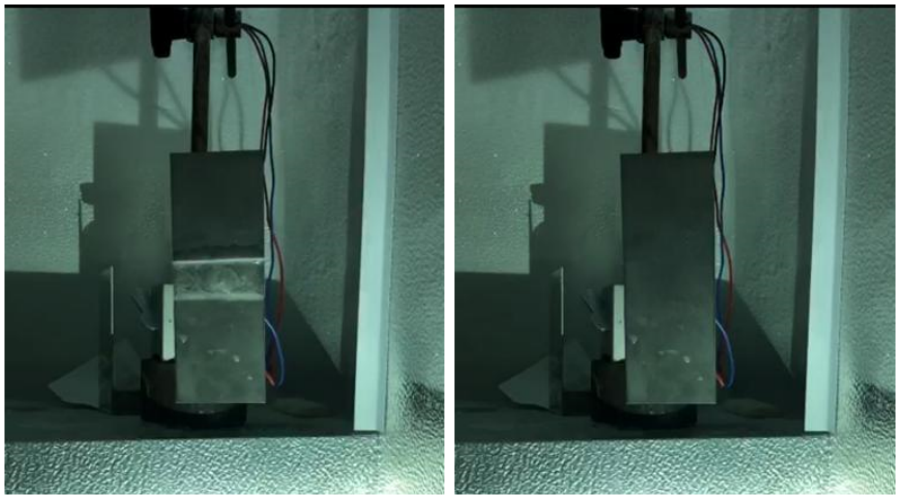

Figure 15 – Example of ice failure for a 25 mm-long ice block using the first flexural mode (200 V)

6.4 Long ice bulk under extensional load

For this configuration, the debonding is expected to initiate cohesively. The experiment results are shown in figure 16. The propagation starts by generating several cohesive cracks on the ice free surface. Then, the adhesive fracture propagation detaches the ice at once.

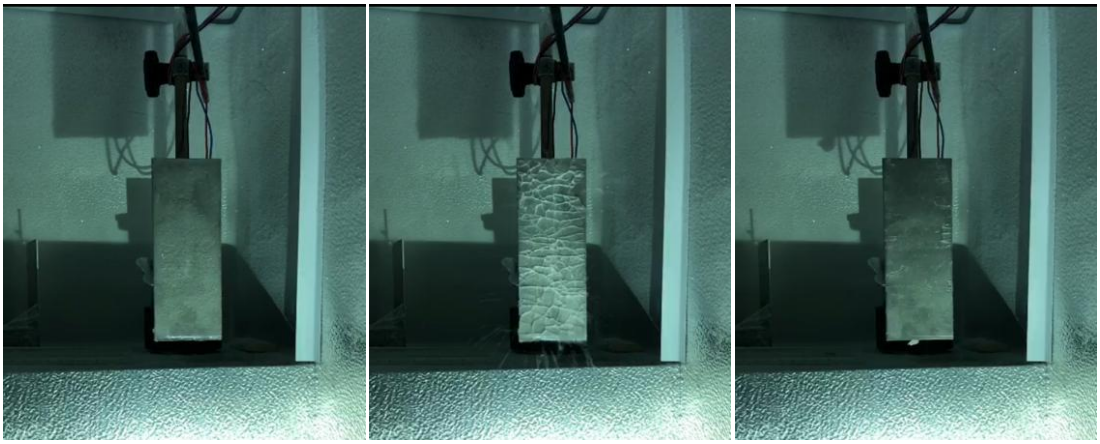

Figure 16 – Example of ice failure with a long ice block using the first extensional mode (200 V)

A numerical study is carried out to explain the presence of multiple cracks. A 3D analysis is run and the results for the first extensional mode exhibit the presence of parasite flexion. As shown in figure 18, at the anti-nodes of the selected mode, the presence of tensile stress concentration is noticed. The amplitudes required to trigger cohesive fractures in the areas presenting major stress concentration are then computed.

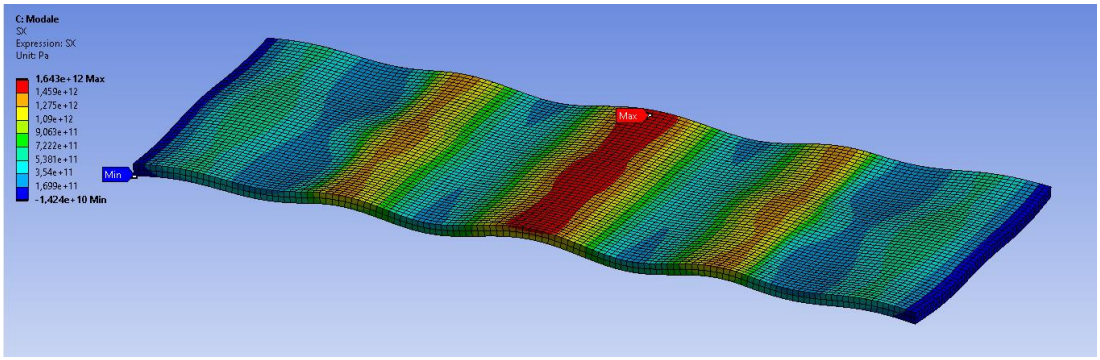

Figure 17 – Tensile stress distribution on the plate

According to the computations, on an undamaged ice layer, the central fracture is firstly generated. Once this crack has occurred, the amplitudes required to initiate cohesive fractures on the sides are easier to reach than the one required to propagate the central crack adhesively. Therefore, the obtained experimental results are supported by numerical tests. The results obtained from the numerical analysis are shown in table 4, where X_τ is the amplitude required to trigger purely adhesive propagation, whereas $X_{\sigma side1}$, $X_{\sigma side2}$ and $X_{\sigma middle}$ are respectively the amplitudes required to initiate a cohesive crack in the leftmost area presenting stress concentration, in the middle-left area, and in the middle of the ice respectively.

Table 4 – Amplitudes required to initiate fractures

	Xτ (m)	X$\sigma_{side1}(m)$	X$\sigma_{side2}(m)$	X$\sigma_{middle}(m)$
Undamaged configuration	$3.32E-05$	$2.98E-05$	$1.5E-05$	$1.15E-05$
Cohesive crack in the middle	$2.33E-05$	$2.14E-05$	$1.56E-05$	-

To further justify why the multitude of cracks sheds instantaneously, the mechanism employed for adhesive fracture propagation is evaluated. To achieve this, one quarter of the plate is modeled and the ice layer covering the surface is divided in several small rectangular blocks to simulate the presence of several cracks.

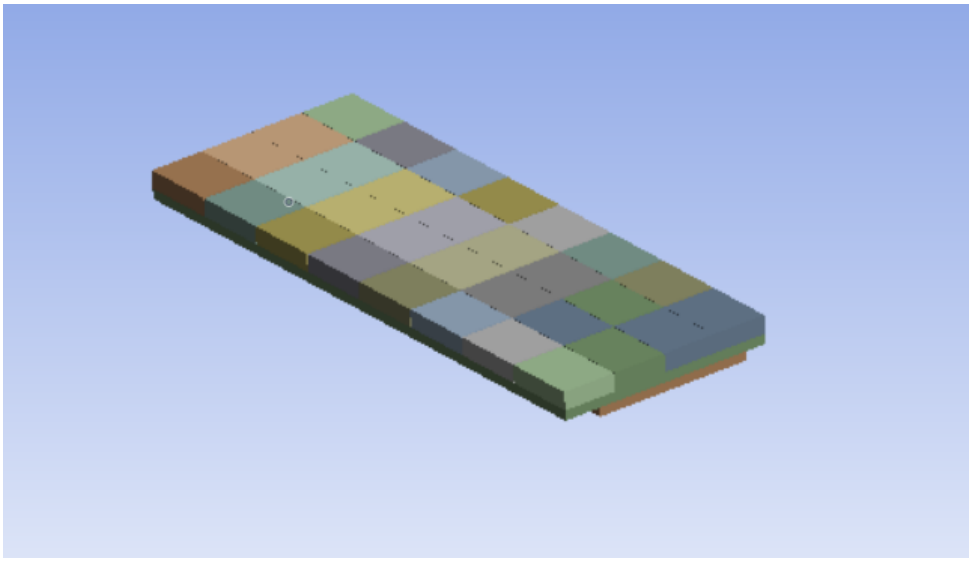

Figure 18 – Plate model used to study ice adhesive separation

The amplitude required to shed the ice using the energy release rate and the shear stress criteria are computed in five selected ice blocks. The results are reported in table 5, and it is possible to notice that the amplitude required to trigger shedding by means of the shear stress criterion are always lower than the one required to propagate with the energy release rate, thus allowing the ice to shed quickly from the substrate.

Table 5 – Amplitudes required to propagate fracture adhesively

X1$_\tau$ (m)	X1$_G$ (m)	X2$_\tau$ (m)	X2$_G$ (m)	X3$_\tau$ (m)
$8.83-06$	$1.90E-05$	$1.02E-05$	$2.20E-05$	$7.45E-06$
X3$_G$ (m)	X4$_\tau$ (m)	X4$_G$ (m)	X5$_\tau$ (m)	X5$_G$ (m)
$1.68E-05$	$1.31E-05$	$3.00E-05$	$1.69E-05$	$5.46E-05$

7. Conclusions

This paper deals with the assessment of the mechanisms of fracture initiation and propagation for electromechanical resonant de-icing systems. Two main ice fracture mechanisms are considered: ini-

tiation by cohesive fracture and adhesive propagation to the edges of the iced structure, and purely adhesive initiation and propagation from the edges to the center. The influence of stress and energy release rate on these phenomena is evaluated. The adopted method consists in computing the amplitudes required to reach the critical mechanical properties of the ice. Through numerical analyses and experimental tests, this technique is proven to accurately predict the de-icing mechanisms, both with flexural and extensional modes. If the structure is largely covered by ice, cohesive fracture occurs first within the ice thickness for both types of resonant modes. Then, the fracture propagates adhesively from the cohesive cracks outwards. Below a certain length of the accreted ice (which is characteristic of each mode), the fracture propagation mechanism becomes purely adhesive at the interface between the ice and the substrate. The study could be effectively extended to other structures and modal shapes, as it can be considered a valuable tool to predict de-icing mechanisms for resonant ice protection systems.

In future studies, the work will focus on the influence of coatings on the fracture mechanisms, thus verifying whether their application on the structure could be beneficial in order to propagate fracture and how the mechanisms of fracture propagation would be different.

8. Contact Author Email Address

mailto: giulia.gastaldo@isae-supaero.fr
mailto: valerian.palanque@isae-supaero.fr

9. Acknowledgments

This project has received funding from the European Union's Horizon 2020 research and innovation programme under the Marie Skłodowska-Curie grant agreement No 956703 (SURFICE Smart surface design for efficient ice protection and control).

10. Copyright Statement

References

[1] Gent, R. W., Dart, N. P., and Cansdale, J. T., "Aircraft icing," *Philosophical Transactions of the Royal Society of London. Series A: Mathematical, Physical and Engineering Sciences*, vol. 358, no. 1776, pp. 2873–2911, 2000.

[2] Cao, Y., Tan, W., and Wu, Z., "Aircraft icing: An ongoing threat to aviation safety," *Aerospace science and technology*, vol. 75, pp. 353–385, 2018.

[3] Lynch, F. T. and Khodadoust, A., "Effects of ice accretions on aircraft aerodynamics," *Progress in Aerospace Sciences*, vol. 37, no. 8, pp. 669–767, 2001.

[4] Meier, O. and Scholz, D., "A handbook method for the estimation of power requirements for electrical de-icing systems," *DLRK, Hamburg*, vol. 31, 2010.

[5] Martin, C. A. and Putt, J. C., "Advanced pneumatic impulse ice protection system (piip) for aircraft," *Journal of Aircraft*, vol. 29, no. 4, pp. 714–716, 1992.

[6] Bai, T., Zhu, C., Miao, B., Li, K., and Zhu, C., "Vibration de-icing method with piezoelectric actuators," *Journal of Vibroengineering*, vol. 17, no. 1, pp. 61–73, 2015.

[7] Villeneuve, E., Harvey, D., Zimcik, D., Aubert, R., and Perron, J., "Piezoelectric deicing system for rotorcraft," *Journal of the American Helicopter Society*, vol. 60, no. 4, pp. 1–12, 2015.

[8] Ramanathan, S., Varadan, V. V., and Varadan, V. K., "Deicing of helicopter blades using piezoelectric actuators," in *Smart Structures and Materials 2000: Smart Electronics and MEMS*, vol. 3990, pp. 281–292, International Society for Optics and Photonics, 2000.

[9] Venna, S. V. and Lin, Y.-J., "Mechatronic development of self-actuating in-flight deicing structures," *IEEE/ASME Transactions on mechatronics*, vol. 11, no. 5, pp. 585–592, 2006.

[10] Venna, S. V., Lin, Y.-J., and Botura, G., "Piezoelectric transducer actuated leading edge de-icing with simultaneous shear and impulse forces," *Journal of Aircraft*, vol. 44, no. 2, pp. 509–515, 2007.

[11] Struggl, S., Korak, J., and Feyrer, C., "A basic approach for wing leading deicing by smart structures," in *Sensors and Smart Structures Technologies for Civil, Mechanical, and Aerospace Systems 2011*, vol. 7981, p. 79815L, International Society for Optics and Photonics, 2011.

[12] Palacios, J., Smith, E., Rose, J., and Royer, R., "Instantaneous de-icing of freezer ice via ultrasonic actuation," *AIAA journal*, vol. 49, no. 6, pp. 1158–1167, 2011.

[13] Palacios, J., Smith, E., Rose, J., and Royer, R., "Ultrasonic de-icing of wind-tunnel impact icing," *Journal of Aircraft*, vol. 48, no. 3, pp. 1020–1027, 2011.

[14] Overmeyer, A., Palacios, J., and Smith, E., "Ultrasonic de-icing bondline design and rotor ice testing," *AIAA journal*, vol. 51, no. 12, pp. 2965–2976, 2013.

[15] Pommier-Budinger, V., Budinger, M., Rouset, P., Dezitter, F., Huet, F., Wetterwald, M., and Bonaccurso, E., "Electromechanical resonant ice protection systems: initiation of fractures with piezoelectric actuators," *AIAA Journal*, vol. 56, no. 11, pp. 4400–4411, 2018.

[16] Sommerwerk, H. and Horst, P., "Analysis of the mechanical behavior of thin ice layers on structures including radial cracking and de-icing," *Engineering Fracture Mechanics*, vol. 182, pp. 400–424, 2017.

[17] Sommerwerk, H., Luplow, T., and Horst, P., "Numerical simulation and validation of electro-impulse de-icing on a leading edge structure," *Theoretical and Applied Fracture Mechanics*, vol. 105, p. 102392, 2020.

[18] Shi, Z., Kang, Z., Xie, Q., Tian, Y., Zhao, Y., and Zhang, J., "Ultrasonic deicing efficiency prediction and validation for a flat deicing system," *Applied Sciences*, vol. 10, no. 19, p. 6640, 2020.

[19] Marbœuf, A., Bennani, L., Budinger, M., and Pommier-Budinger, V., "Electromechanical resonant ice protection systems: numerical investigation through a phase-field mixed adhesive/brittle fracture model," *Engineering Fracture Mechanics*, vol. 230, p. 106926, 2020.

[20] Budinger, M., Pommier-Budinger, V., Bennani, L., Rouset, P., Bonaccurso, E., and Dezitter, F., "Electromechanical resonant ice protection systems: analysis of fracture propagation mechanisms," *AIAA Journal*, vol. 56, no. 11, pp. 4412–4422, 2018.

[21] Leguillon, D., "Strength or toughness? a criterion for crack onset at a notch," *European Journal of Mechanics-A/Solids*, vol. 21, no. 1, pp. 61–72, 2002.

[22] Martin, E., Vandellos, T., Leguillon, D., and Carrère, N., "Initiation of edge debonding: coupled criterion versus cohesive zone model," *International Journal of Fracture*, vol. 199, no. 2, pp. 157–168, 2016.

[23] Golovin, K., Dhyani, A., Thouless, M., and Tuteja, A., "Low–interfacial toughness materials for effective large-scale deicing," *Science*, vol. 364, no. 6438, pp. 371–375, 2019.

[24] Liu, Y., Xi, N., Zhang, X., and Liu, N., "Study of atmospheric ice adhesion properties of superhydrophobic surface by in-situ shear system," *Materials Express*, vol. 10, no. 10, pp. 1704–1710, 2020.

[25] Chu, M. C. and Scavuzzo, R. J., "Adhesive shear strength of impact ice," *AIAA Journal*, vol. 29, pp. 1921–1926, Nov. 1991.

[26] Tryde, P., ed., *Physics and Mechanics of Ice: Symposium Copenhagen, August 6–10, 1979, Technical University of Denmark*. Berlin, Heidelberg: Springer Berlin Heidelberg, 1980.

[27] Frederking, R., Svec, O., and Timco, G., "On Measuring the shear strength of ice," Jan. 2010.

[28] Rønneberg, S., Laforte, C., Volat, C., He, J., and Zhang, Z., "The effect of ice type on ice adhesion," *AIP advances*, vol. 9, no. 5, p. 055304, 2019.

[29] Andrews, E. H. and Lockington, N. A., "The cohesive and adhesive strength of ice," *Journal of Materials Science*, vol. 18, pp. 1455–1465, May 1983.

[30] Meng, W. and Guo, Y., "Experimental Study on Mechanical Properties of Ice," p. 5.

[31] Petrovic, J. J., "Review Mechanical properties of ice and snow," p. 6.

[32] Druez, J., Nguyen, D., and Lavoie, Y., "Mechanical properties of atmospheric ice," *Cold Regions Science and Technology*, vol. 13, pp. 67–74, Oct. 1986.

[33] Reich, A., Scavuzzo, R., and Chu, M., "Survey of mechanical properties of impact ice," in *32nd Aerospace Sciences Meeting and Exhibit*, (Reno,NV,U.S.A.), American Institute of Aeronautics and Astronautics, Jan. 1994.

[34] Huang, X., Tepylo, N., Pommier-Budinger, V., Budinger, M., Bonaccurso, E., Villedieu, P., and Bennani, L., "A survey of icephobic coatings and their potential use in a hybrid coating/active ice protection system for aerospace applications," *Progress in Aerospace Sciences*, vol. 105, pp. 74–97, Feb. 2019.

[35] Budinger, M., Pommier-Budinger, V., Reysset, A., and Palanque, V., "Electromechanical Resonant Ice Protection Systems: Energetic and Power Considerations," *AIAA Journal*, vol. 59, no. 7, pp. 2590–2602, 2021. Publisher: American Institute of Aeronautics and Astronautics _eprint: https://doi.org/10.2514/1.J060008.

[36] Palanque, V., Marbœuf, A., Budinger, M., Pommier-Budinger, V., and Bennani, L., "Improving mechanical ice protection systems with substrate thickness and topology optimization," *In preparation*, 2021.